Eleventh International Conference on CFD in the Minerals and Process Industries
CSIRO, Melbourne, Australia
7-9 December 2015

INVESTIGATING THE FEASIBILITY OF IMPLEMENTING STEADY RELATIVE TO PULSATILE FLOW IN ATHEROSCLEROSIS GROWTH MODELING

Sargon A. GABRIEL[1*], Si-Zhong LU[1], Yan DING[1], Yuqing FENG[2] and John A. GEAR[1]

[1] School of Mathematical and Geospatial Sciences, RMIT University, Victoria 3001, AUSTRALIA
[2] CSIRO Minerals Resources Flagship, Clayton, Victoria 3169, AUSTRALIA
*Corresponding author, E-mail address: sargon.gabriel@rmit.edu.au

ABSTRACT

Atherosclerosis is a cardiovascular disease, characterized by the development of blood flow impeding lesions within arterial walls. The progression of the disease is primarily governed by an inflammatory process, which itself is driven by the transport of multiple biochemical species from the blood flow into the arterial wall. As a dominant driver for mass transport, pulsatile blood flow conforms to time-scales considerably smaller than those of atherosclerosis growth. Due to the complexity involved in resolving both time-scales, standard mathematical models for describing the growth and progression of atherosclerosis have thus far ignored flow pulsatility. However, it is now understood that this assumption fails for complex flow-fields. The present study attempts to quantify the extent to which a steady flow may be used in atherosclerosis growth models. Using an idealised arterial bifurcation, both steady-state and pulsatile flows are compared. A simplified atherosclerosis growth model is further implemented on the steady flow, to identify sites predisposed to the emergence of atherosclerosis, and their relative extent to which growth occurs. Through the implementation of a pulsatile-perturbation kinetic energy quotient, it was found that sites which were predisposed to atherosclerosis growth were also incidentally coincident with those which were most disturbed by flow pulsatility.

NOMENCLATURE

d	inlet diameter	P	period count
D	diffusion coefficient	Pe	Péclet number
f_g	growth scale factor	R	residual
J	flux	Re	Reynolds number
k	porosity	S	source term
m, n	counter variables	t	time
n	unit normal	T	time period length
N	iteration limit	u	fluid velocity
p	pressure	x	spatial position
$\dot{\gamma}$	strain-rate	μ	dynamic viscosity
Γ	domain boundary	ρ	density
∂	partial derivative	τ_w	wall shear stress
δ_{ij}	Kronecker delta	ϕ, φ	scalar variable
κ	kinetic energy	ψ	flux aggregate
λ	κ quotient	Ω	domain

Note with Nomenclature:

The subscripts $i, j, k \in \{1, 2, 3\}$ are reserved for tensor index notation; all other subscripts are for designating variables, and should not be used as tensor indices.

INTRODUCTION

The development of atherosclerosis is primarily governed by an inflammatory process within the arterial wall, which is itself driven by mass transport of participating species. If left untreated, the disease may develop to severely retard blood flow, causing pressure losses or else impeded flow transport, which may result in ischemia and eventual infarction of downstream tissue. Should the downstream tissue be critical to the function of the body, the outcome may be manifest in life-threatening diseases such as stroke or coronary artery disease; both of which represent the leading cause of mortality worldwide (Libby, 2012).

The inflammatory process governing atherosclerosis involves the transport of multiple biological and chemical species, which are predominantly convected by the blood flow-field (Chatzizisis et al, 2007). However, as blood flow is characterized by periodic fluctuations arising from the rhythmic beating of the heart, so too is the transport of these species. The processes describing the progression of atherosclerosis are therefore found to conform to two dominant time-scales; one of which governs the pulsatility of the blood flow-field and hence mass transport, and the other governing the relatively monotonic progression of the inflammatory process and hence lesion growth.

In effort to better understand the disease, mathematical models have been developed to characterize the growth behaviour of atherosclerosis (Cilla et al, 2014; Díaz-Zuccarini et al, 2014). The purpose of such models is to provide a framework by which the nature and growth behaviour of the disease may be analysed in a controlled computational environment, thereby allowing for the development of treatment methods to control the rate of progression and eventually reversal of the disease.

Unfortunately, due to the lack of available data or else sufficient understanding of the precise mechanics governing atherosclerosis, such models generally make significant assumptions to bypass these difficulties. One characteristic assumption, common to the majority of present growth models, is that the pulsatile nature of blood flow is ignored and the flow-field is treated as steady (Cilla et al, 2014; Díaz-Zuccarini et al, 2014; Filipovic et al, 2013; Gessaghi et al, 2011; Calvez et al, 2010). The reason often cited is that since the time-scale associated with pulsatile flow is significantly shorter than that of lesion growth, it may be assumed to have no significant role on the growing lesion, and so may be safely ignored (Calvez et al, 2010).

However in ignoring the pulsatility of the flow, the effect that it has on mass-transport and subsequent atherosclerosis growth is not accounted for. In effort to investigate this influence, the authors conducted a study to compare pulsatile and equivalent steady-state flow-fields (Gabriel et al, 2014). A result of the study is presented in figure 1, depicting the comparison between a period-averaged pulsatile (PAP) flow-field and its equivalent steady-state (SS) flow-field within a symmetric two-dimensional arterial bifurcation. At region 1 of the figure, where the flow is not disturbed, both flow types display identical behaviour. However, at the site of bifurcation, where recirculation zones form, there is a marked difference between the two figures; in that the steady flow does not reveal the temporally varying nature of the recirculation zones, leading to dissimilarities between the two flow-fields at regions 2 and 3. These variations incidentally coincide within the vicinity of the arterial bifurcation, which is a site generally associated with vulnerability to the development of atherosclerosis (Chatzizisis et al, 2007).

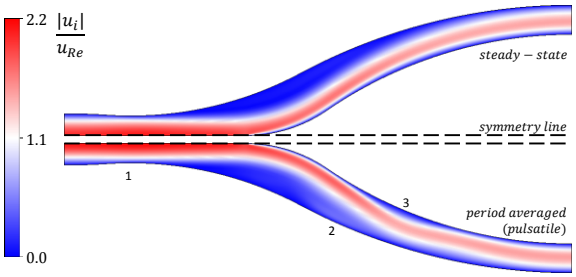

Figure 1: Velocity magnitude flow-field comparison for a PAP and equivalent SS flow in a symmetric two-dimensional arterial bifurcation (Gabriel et al, 2014).

In their study on the effect of pulsatile blood flow on species transport into the arterial wall, Liu et al (2011) also reported the differences between the two flow-fields resulted by steady-state and pulsatile flows. They noted that the differences between the two flow-fields may manifest in the resulting flow-convected species transport. The flow-field results from the authors' previous study (Gabriel et al, 2014) was in a very good agreement with the findings of Liu et al (2011). Consequently the authors believe that using a steady flow state flow and ignoring the pulsatility may not be appropriate to accurately model atherosclerosis; since the near-wall transport of species, which contribute to the development of atherosclerosis, would be influenced by the presence of time-varying flow features, such as recirculation-zones (Chatzizisis et al, 2007), thereby directly influencing the growth of atherosclerosis.

The present study attempts to investigate the validity of this claim by assessing the extent of deviation between the two flow-fields. This is realized by evaluating the extent of spatial coincidence amongst sites that exhibit significant discrepancy between the two flow-fields and those prone to the emergence of atherosclerosis. The former is achieved by the comparative assessment of flow-derived statistics, and the later through the implementation of a simplified atherosclerosis growth model.

MODEL DESCRIPTION

In the following assessment, we maintain the assumption that the arterial wall remains fixed throughout a period. We begin by defining the dimensionless parameters of the governing equations; the Reynolds number Re is defined as the ratio of inertial to diffusive forces of the flow, and similarly the Péclet number Pe as the ratio of the rate of inertial to diffusive transport of a scalar quantity:

$$Re = \frac{\rho u_{Re} d}{\mu} \quad , \qquad Pe = \frac{u_{Re} d}{D} \tag{1}$$

where u_{Re} is the PAP/SS mean inflow velocity magnitude. Depending on the flow Reynolds number, arterial bifurcations may be host sites to the formation of recirculating-flow zones, which are generally characterized by low-velocity flow and hence low wall shear stress (WSS). This predisposes the sites to vulnerability for the formation of atherosclerosis (Libby, 2012); since amongst other factors, the continuous endothelial production of the anti-inflammatory agent nitric-oxide (NO) is disrupted by low endothelial shear stress (ESS) (Chatzizisis et al, 2007).

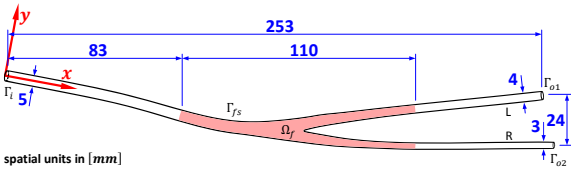

Figure 2: Schematic diagram of arterial bifurcation with flow extensions included; region of interest is shaded.

For the present study, an idealized three-dimensional arterial bifurcation, modelled on a carotid artery with inflow diameter of $d = 5\ [mm]$, is selected (refer to figure 2). To reduce the effect of three-dimensional variations in the geometry, it is set to be symmetric about the x-y plane, though the bifurcation itself is asymmetric in the plane.

Flow Physics

The role of blood flow is twofold with respect to atherosclerosis. Firstly, it is the dominant convective transport within the lumen Ω_f of species that participate in the inflammatory process driving atherosclerosis. And secondly, it is integral to the determination of ESS, which is a governing variable by which endothelial cells respond to facilitate species transport into the arterial wall; such as that of lipoproteins, which are integral to the inflammatory process governing atherosclerosis (Chatzizisis et al, 2007).

For the present study, blood flow is modelled by the incompressible mass and momentum conservation (Navier-Stokes) equations for a Newtonian fluid:

$$\partial_i u_i = 0 \tag{2}$$

$$\rho\left(\partial_t + u_j \partial_j\right) u_i - \mu \partial_j \partial_j u_i = -\partial_i p \tag{3}$$

Blood is treated as a homogenous fluid with isotropic properties, where standard values of blood density and approximate Newtonian viscosity are respectively assigned as $\rho = 1050\ [kg/m^3]$ and $\mu = 3.5 \times 10^{-3}\ [kg/m/s]$ (Cilla et al, 2014). The state of complexity of the flow equations is sufficient for a rudimentary approximation to the flow physics governing atherosclerosis. As this is the case for the present study, where a simple flow-field is required, greater complexity is not needed. However, the authors wish to note that appropriate blood viscosity and turbulence models need be applied for blood flow models in general. This is particularly important when

atherosclerosis or near-wall mass transport is involved, since the presence of atherosclerosis lesions will contribute to the generation of turbulent kinetic energy that would influence the flow-field (Chatzizisis et al, 2007; Cilla et al, 2014). Furthermore, the accurate evaluation of the WSS, is integral to the development of these lesions. Therefore, the assumption of constant viscosity for medium to large sized arteries, may be satisfactory for the bulk flow, though inappropriate in the near-wall regions where the WSS and mass transport are important.

Boundary conditions of the flow equations are set to be consistent between the PAP case and its SS equivalent, so that comparison between the two may be made. Therefore for the PAP flow case, a uniform Dirichlet condition of inflow volumetric flow-rate waveform (refer to figure 3) is assigned to Γ_i, and its period-averaged value is assigned for the SS equivalent case. Furthermore, to maintain relative similarity in flow behaviour to carotid bifurcations, the outlet boundaries Γ_{o1} and Γ_{o2} have been selectively set to a 0.7:0.3 respective flow share. At the wall boundary Γ_{fs}, a no-slip boundary condition $u_i = 0$, is assigned.

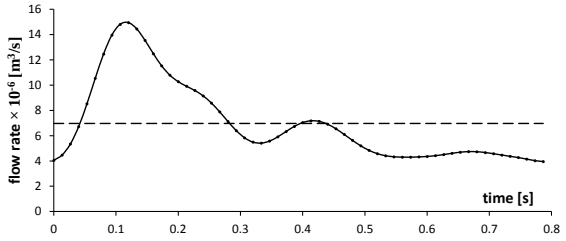

Figure 3: Pulsatile volumetric inflow-rate waveform and steady-state period-averaged equivalent (Dong et al, 2013).

Flow-derived Statistics

To investigate the pulsatile flow-field for comparison to its SS equivalent, various flow-statistics are employed to extract meaningful data in a period-averaged sense. We begin by defining a representative scalar variable φ, that is transported within pulsatile blood flow of period-length T_p:

$$\varphi \equiv \{\varphi(x_i, t_p) \quad | \quad t_p \in T_p\}$$

Within an Eulerian reference frame, the transported value of φ may be decomposed into its periodic-mean $\overline{\varphi}$ and time-dependant perturbation φ'. Following Reynolds-decomposition, the variable φ may be defined as:

$$\varphi(x_i, t_p) = \overline{\varphi}(x_i) + \varphi'(x_i, t_p) \tag{4}$$

$$\overline{\varphi}(x_i) = \frac{1}{T_p}\int_{T_p} \varphi(x_i, t_p)\, dt_p \tag{5}$$

Using this definition, the velocity vector u_i may be treated in the same way, such that:

$$u_i = \overline{u_i} + u_i' \tag{6}$$

From this, the PAP kinetic energy of the mean flow and its perturbations may be respectively defined as:

$$\kappa_{\overline{u}} = \tfrac{1}{2}\,\overline{u_i}\,\overline{u_i} \tag{7}$$

$$\kappa_{u'} = \tfrac{1}{2}\,\overline{u_i'\,u_i'} \tag{8}$$

which may be used to define the quotient of these quantities λ_u, as a measure of the local influence of pulsatile perturbations relative to the mean flow.

$$\lambda_u = \kappa_{u'}/\kappa_{\overline{u}} \tag{9}$$

Furthermore, definitions (4) and (5) may also be applied to both the WSS vector τ_{w_i} and its magnitude τ_w, to obtain:

$$\overline{\tau_{w_i}} = \frac{1}{T_p}\int_{T_p} \tau_{w_i}\, dt_p \tag{10}$$

$$\overline{\tau_w} = \frac{1}{T_p}\int_{T_p} |\tau_{w_i}|\, dt_p \tag{11}$$

which may be used to define the oscillatory shear index OSI, a useful statistic for measuring the extent of the local deviation of the WSS from its period-mean value (Ku et al, 1985; Liu et al, 2011).

$$OSI = \frac{1}{2}\left(1 - \frac{\left|\overline{\tau_{w_i}}\right|}{\overline{\tau_w}}\right) \tag{12}$$

Additionally, to identify sites predisposed to flow-shearing, the strain-rate $\dot{\gamma}$ is used:

$$\dot{\gamma} = \sqrt{\tfrac{1}{2}\dot{\gamma}_{ij}\dot{\gamma}_{ij}} \quad , \qquad \dot{\gamma}_{ij} = \partial_i u_j + \partial_j u_i \tag{13}$$

Simple Atherosclerosis Growth

For the evaluation of the spatial distribution of sites prone to the emergence of atherosclerosis and to obtain a measure of their relative growth extent, a simplified atherosclerosis growth model is implemented. The reader is advised that the present study is not intended for the development of a growth model, but rather towards the understanding of the scope of validity that a SS flow-field may represent a pulsatile flow in atherosclerosis growth models. For current-state spatiotemporal growth models, the reader is advised to consult the papers by Cilla et al (2014), Díaz-Zuccarini et al (2014), Filipovic et al (2013), Gessaghi et al (2011) and Calvez et al (2010) amongst others.

To reduce interference from other non-flow physics, the present growth model is modified from the above stated models, to the extent that the effects of flow physics become the dominant driver for atherosclerosis growth. This is achieved by omitting the arterial wall domain (refer to figure 2) and treating its interfacial boundary Γ_{fs} by equivalent flux-balance boundary conditions of low-density lipoproteins (LDL), a dominant species integral to the development of atherosclerosis (Libby, 2012).

The mass transport of species is modelled via scalar transport equations. In conservative form, the general transport equation for a passive scalar variable ϕ with source term S, is given as follows:

$$\partial_t \phi + \partial_i\left(u_i\phi - D_{ij}\partial_j\phi\right) = S \tag{14}$$

For many of the species involved in atherosclerosis, their diffusion coefficients are generally isotropic within the blood medium, which may be set into equation (14) by casting $D_{ij} = D\delta_{ij}$, where D is the isotropic diffusion

coefficient. At the inflow boundary Γ_i, a uniform Dirichlet condition is assigned for the scalar. Whereas at the outflow boundaries Γ_{o1} and Γ_{o2}, a zero flux condition is assigned $n_i \partial_i \phi = 0$. For the wall boundary Γ_{fs}, a flux balance boundary condition is assigned, as denoted by equation (15), where J_ϕ is the net scalar flux into the boundary; for the present study $J_\phi = k\phi$, where k is a bulk permeability to the scalar ϕ.

$$J_u \phi - n_i D_{ij} \partial_j \phi = J_\phi \qquad (15)$$

For the present model, growth is implemented as a surface-normal displacement on Γ_{fs}, arising due to net mass flux of low density lipoprotein (LDL) species ϕ_{LDL}, which exceed a threshold limit J_{ϕ_0}. This is described by equations (16) and (17), which denote the displacement of a material point x_i on the surface Γ_{fs} by the normalized flux aggregate ψ of LDL species. The corresponding growth is scaled by a factor f_g, such that the maximum displacement during the integer iteration m is f_g.

$$x_i^{m+1} = x_i^m + f_g \, \psi(\phi_{LDL})^m \, n_i^m \qquad (16)$$

$$\psi(\phi) = \frac{\max\{J_\phi - J_{\phi_0}, 0\}}{\max_{\Gamma_{fs}}\{\max\{J_\phi - J_{\phi_0}, 0\}\}} \qquad (17)$$

LDL inflow into the domain is defined via a normalised Dirichlet condition of $\phi_{LDL} = 1$, assigned at the inlet Γ_i. The diffusive coefficient of LDL in blood is represented by the isotropic approximation of $D = 5.0 \times 10^{-12}\ [m^2/s]$ (Stangeby and Ethier, 2002). For the present assessment, wall fluxes are treated as constant, such that $J_u = 1.78 \times 10^{-8}\ [m/s]$ (Meyer et al, 1996) and $k = 2.0 \times 10^{-10}\ [m/s]$ (Stangeby and Ethier, 2002). Due to the wall-less approach presented for the growth model, closure for the scalar transport equations at the wall boundary cannot be realised. Thus to address this limitation, a mass-aggregate cut-off flux of $J_{LDL_0} = 1.1k$ is assigned.

The growth model is phenomenological in principle, and is inherently not mass conservative with respect to the growing lesion. However, for the objectives of the present study, it is sufficient to determine a satisfactory approximation to the spatial distribution of atherosclerosis lesions. Furthermore, it is implemented on a steady flow-field, since it is presently computationally prohibitive to directly implement the growth model on a pulsatile flow-field. This is due to the time-scale associated with growth of a lesion being orders of magnitude greater than the length of a cardiac period (Di Tomaso et al, 2015; Waters et al, 2011). Studies are being presently conducted by the authors to bypass these limitations via the development of models to represent the pulsatile flow-field within growth models. Nevertheless, since the SS and PAP flow-fields are generally approximately alike, then a steady flow-field may be argued to be sufficient for an approximate evaluation of the sites of emergence of atherosclerosis, though the corresponding growth behaviour may differ.

Computational Implementation

The above models were implemented into a computational framework, with the cell-centred finite-volume solver ANSYS Fluent v14.5 as the principal solver. For the arterial bifurcation geometry of figure 2, a hybrid mesh was constructed; where swept hexahedral elements were constructed on the tubular segments of the geometry and tetrahedral/prismic elements at the bifurcation site to serve as a buffer region between the hexahedral mesh zones (refer to figure 4). Following mesh convergence, the final mesh employed for this study required 3.24×10^5 elements.

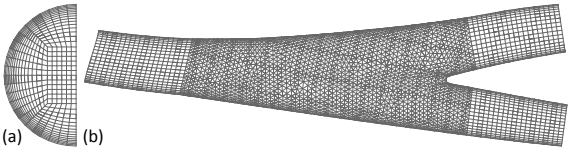

Figure 4: Mesh of the arterial geometry, denoting the (a) cross-section mesh of the tubular segments of the geometry, and the (b) hybrid buffer mesh at the bifurcation.

Pressure-velocity coupling for the Navier-Stokes equations was implemented via the SIMPLE algorithm. Spatial discretization of the momentum (flow) variables was made via a second-order upwind scheme, and for the pressure, a neighbour-cell interpolation scheme, using momentum-equation coefficient weighting (referred as the 'standard' scheme in ANSYS Fluent). For the scalar transport equation, a first-order upwind scheme was implemented, to avoid numerical instabilities arising due to the high Péclet numbers associated with LDL transport; higher order scheme implementation is being presently investigated. Spatial discretization of field-variable gradients was made via least-squares cell-based interpolation.

For transient flows, time-stepping was attained via an implicit first-order forward-differencing scheme. However, for the atherosclerosis growth model, a pseudo-steady method was adopted, where an iterative scheme was implemented in place of a time-scale. This is summarised by figure 5 below.

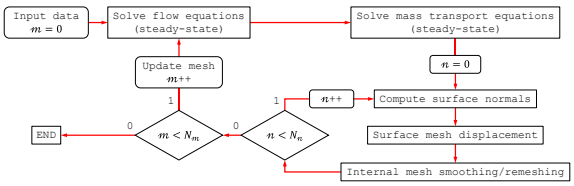

Figure 5: Iterative growth algorithm.

Following the growth algorithm, an inner growth loop is performed on the domain N_n times and an outer loop on the updated equations N_m times. For the present setting, the iterative loop limits are set to $N_m = 20$ and $N_n = 20$. Since mass aggregate is not conserved with the elimination of the arterial wall, then a time-scale is not realizable. To derive a comparable measure for elapsed time, the integer iteration count m is employed, such that growth within each m iteration is normalized, to give a maximum surface growth of magnitude $f_g = 5.0 \times 10^{-3}\ [mm]$. Growth of surface nodes is made via an explicit nodal displacement. Therefore to overcome skewness of volumetric cells within Ω_f after surface displacements on Γ_{fs}, a spring-based smoothing operation is performed on cell nodes within Ω_f.

For the pulsatile flow case, it is necessary to purge the flow-field from association with initial conditions before meaningful results may be extracted. Therefore, to evaluate the number of periods P required to accomplish this, a residual function $R_{\overline{u}}$ was developed (refer to equation (18)).

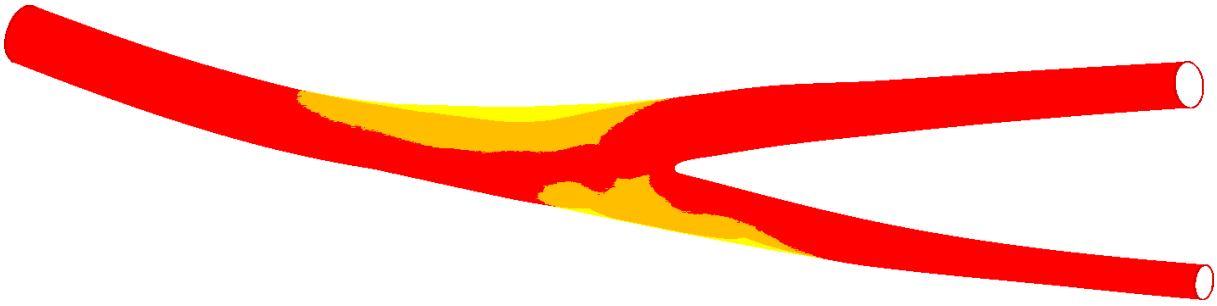

Figure 6: Rendering of computed atherosclerosis distribution (yellow) on arterial bifurcation surface (red).

It was observed that by setting $R_{\overline{u}} < 10^{-7}$, in general 3-4 periods were required to purge the flow from resting-state initial conditions.

$$R_{\overline{u}} = \left| \left[\int_{\Omega_f} |\overline{u}| \, d\Omega_f \Big/ \int_{\Omega_f} u_{Re} \, d\Omega_f \right]_{P=m}^{m+1} \right| \qquad (18)$$

RESULTS AND DISCUSSION

The SS flow case is equivalent to applying period-averaging to the boundary-conditions alone, and not the domain equations. Therefore, it is expected that a close though not identical resemblance be observed with PAP results. This is perceived in the flow-field distributions of figure 7; where the PAP and SS flows are similar, except for a difference within the vicinity of the bifurcation, which appears to coincide with boundaries of recirculation zones. This indicates that whilst the SS flow captures most flow features of the PAP, it fails to accurately represent their time-varying behaviour, particularly for recirculation zones, whose size may temporally vary throughout a period.

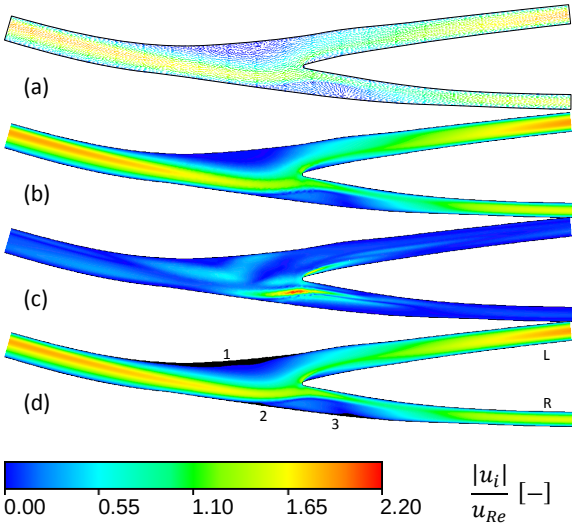

Figure 7: Flow-field distribution on x-y symmetry-plane; (a) SS vector plot (b) SS contour (c) PAP/SS difference scaled × 5 contour (d) post-growth SS contour.

Following the action of atherosclerosis growth on the arterial bifurcation, the resulting lesion distribution is evaluated and displayed in contrast to its original state in figures 6 and 7. The resulting lesions are observed to coincide with sites of recirculation zones, which follows the documented observation that atherosclerosis lesions highly correlate with regions of low ESS (Chatzizisis et al, 2007). Furthermore, a relatively large lesion occurs upstream to branch L, at region 1 of the bifurcation. From the flow-field distribution in figure 7, it is perceived that the lesion corresponds to the site of the dominant recirculating-flow zone at the bifurcation. That this lesion coincides well with the recirculation zone, indicates that it is important to appreciably resolve the recirculation zone behaviour.

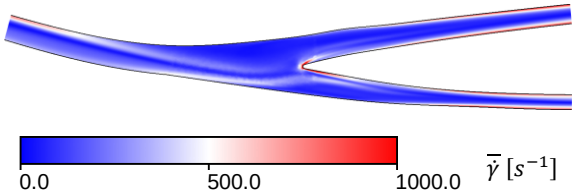

Figure 8: Period-averaged strain-rate distribution on x-y symmetry-plane.

Other lesions are also apparent at sites upstream to branch R, at regions 2 and 3 of figure 7. These lesions correspond to the secondary recirculation zone at that site and are closer to the bifurcation zone than the larger lesion. From a physiological perspective, the close proximity of these lesions to the bifurcation zone and arterial branches of smaller diameter, poses a risk to potential blockage of the artery. This outcome is further enhanced by the presence of high shear flows at the site (refer to figure 8), which upon significant stressing of the upstream wall of the R branch, may potentially result in wall fracture or thrombosis. This further signifies the need to resolve the pulsatile flow when implementing an atherosclerosis growth model, since an incorrect resolution of the location of a lesion may lead to potentially differing physiological outcomes.

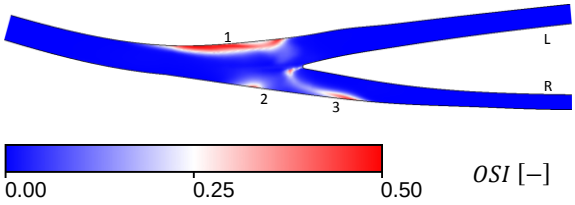

Figure 9: Oscillatory shear index contour plot on wall Γ_{fs}.

Observations of the oscillatory shear index plot in figure 9 indicate that the OSI distribution coincides well with that of the computed atherosclerosis growth distribution. Since the OSI is a well-regarded marker for potential development of atherosclerosis (Ku et al, 1985; Liu et al, 2011), it is deduced from this particular study, that using a steady inflow model for growth may be sufficient for a qualitative assessment of spatial growth distributions. However, for a quantitative understanding of the growth behaviour, the same conclusion cannot be deduced at the present, since

further studies and results are required to verify this, particularly for long-term growth predictions.

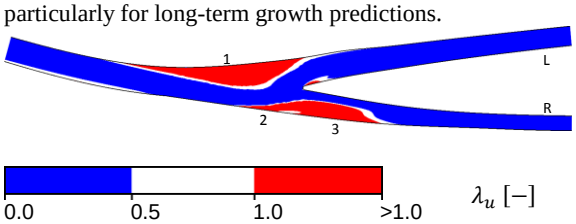

Figure 10: Kinetic-energy quotient contour plot of pulsatile perturbations on x-y symmetry-plane.

To indicate regions most-affected by flow pulsatility, the pulsatile-perturbation kinetic energy quotient λ_u is used. As the flow's pulsatility is proportional to the inflow's amplitude about its mean, it is deduced that as the inflow amplitude tends away from zero, then so too would the quotient λ_u. Regions that have $\lambda_u > 1$ indicate that the pulsatile perturbation kinetic energy is greater than that of the mean flow, and so would be identified as most prone to influence by flow pulsatility. It is observed from the λ_u plot in figure 10, that the sites most affected by flow pulsatility also encompass regions of observed atherosclerosis growth. This observation, indicates that flow pulsatility may contribute to lesion growth behaviour, since the effects of flow pulsatility appear to be incidentally most influential at sites of observed growth. However, to verify this deduction further studies need be performed, particularly with respect to validation with an atherosclerosis growth model which integrates the effects of flow pulsatility.

CONCLUSION

The premise of using a steady-inflow condition in atherosclerosis growth modelling has been investigated in this study. Comparison of period-averaged pulsatile flow to that of the equivalent steady-state flow reveal that the two flow-fields are generally similar, indicating that steady-inflow growth models may be satisfactory for qualitative assessment of spatial growth distributions. However, comparison of pulsatile flow markers, such as the oscillatory shear index and pulsatile-perturbation kinetic energy quotient, to that of growth results from a simple atherosclerosis growth model, indicate that sites apparently predisposed to the emergence of atherosclerosis, were generally coincident with those most influenced by flow pulsatility. This suggests that lesion growth behaviour at these sites may be influenced by flow pulsatility, though further studies are required to verify this claim.

ACKNOWLEDGEMENTS

This research was supported by an Australian Postgraduate Award and a grant from the CSIRO, through the ATN Industry Doctoral Training Centre.

REFERENCES

CALVEZ, V., HOUOT, J.G., MEUNIER, N., RAOULT, A. and RUSNAKOVA, G., (2010), "Mathematical and numerical modeling of early atherosclerotic lesions", ESAIM: Proceedings, **30**, 1-14.

CHATZIZISIS, Y.S., COSKUN, A.U., JONAS, M., EDELMAN, E.R., FELDMAN, C.L. and STONE, P.H., (2007), "Role of endothelial shear stress in the natural history of coronary atherosclerosis and vascular remodeling: molecular, cellular, and vascular behavior", Journal of the American College of Cardiology, **49**, 2379-2393.

CILLA, M., PEÑA, E. and MARTÍNEZ, M.A., (2014), "Mathematical modelling of atheroma plaque formation and development in coronary arteries", Journal of the Royal Society: Interface, **11**, 1-16.

DÍAZ-ZUCCARINI, V., DI TOMASO, G., AGU, O. and PICHARDO-ALMARZA, C., (2014), "Towards personalised management of atherosclerosis via computational models in vascular clinics: technology based on patient-specific simulation approach", Healthcare Technology Letters, **1**, 13-18.

DI TOMASO, G., PICHARDO-ALMARZA, C., AGU, O. and DÍAZ-ZUCCARINI, V., (2015), "A multiscale and patient-specific computational framework of atherosclerosis formation and progression: a case study in the aorta and peripheral arteries", Procedia Computer Science, **51**, 1118-1127.

DONG, J., INTHAVONG, K. and TU, J., (2013), "Image-based computational hemodynamics evaluation of atherosclerotic carotid bifurcation models", Computers in Biology and Medicine, 43, 1353-1362.

FILIPOVIC, N., TENG, Z., RADOVIC, M., SAVELJIC, I., FOTIADIS, D. and PARODI, O., (2013), "Computer simulation of three-dimensional plaque formation and progression in the carotid artery", Medical & biological engineering & computing, **6**, 607-616.

GABRIEL, S.A., DING, Y., FENG, Y. and GEAR, J.A., (2014), "Comparative analysis of pulsatile and steady flow on arterial mass transport", 19th Australasian Fluid Mechanics Conference.

GESSAGHI, V.C., RASCHI, M.A., TANONI, D.Y., PERAZZO, C.A. and LARRETEGUY, A.E., (2011), "Growth model for cholesterol accumulation in the wall of a simplified 3D geometry of the carotid bifurcation", Computer Methods in Applied Mechanics and Engineering, **200**, 2117-2125.

KU, D.N., GIDDENS, D.P., ZARINS, C.K. and GLAGOV, S., (1985), "Pulsatile flow and atherosclerosis in the human carotid bifurcation. Positive correlation between plaque location and low oscillating shear stress", Arteriosclerosis, thrombosis, and vascular biology, **5**, 293-302.

LIBBY, P., (2012), "Inflammation in atherosclerosis", Arteriosclerosis, thrombosis, and vascular biology, **32**, 2045-2051.

LIU, X., FAN, Y., DENG, X. and ZHAN, F., (2011), "Effect of non-Newtonian and pulsatile blood flow on mass transport in the human aorta", Journal of biomechanics, **44**, 1123-1131.

MEYER, G., MERVAL, R. and TEDGUI, A., (1996), "Effects of pressure-induced stretch and convection on LDL and albumin uptake in the rabbit aortic wall. Circulation research", **79**, 532-540.

STANGEBY, D.K. and ETHIER, C.R., (2002), "Computational analysis of coupled blood-wall arterial LDL transport", Journal of biomechanical engineering, **124**, 1-8.

WATERS, S.L., ALASTRUEY, J., BEARD, D.A., BOVENDEERD, P.H.M., DAVIES, P.F., JAYARAMAN, G., JENSEN, O.E., LEE, J., PARKER, K.H., POPEL, A.S., SECOMB, T.W., SIEBES, M., SHERWIN, S.J., SHIPLEY, R.J., SMITH, N.P. and VAN DE VOSSE, F.N., (2011), "Theoretical models for coronary vascular biomechanics: progress & challenges", Progress in biophysics and molecular biology, **104**, 49-76.